Observing gravitational wave polarizations with the LISA-TAIJI network

Gang Wang[1,†] and Wen-Biao Han[1,2,3,4,5,*]

[1]*Shanghai Astronomical Observatory, Chinese Academy of Sciences, Shanghai 200030, China*
[2]*School of Astronomy and Space Science, University of Chinese Academy of Sciences, Beijing 100049, China*
[3]*School of Fundamental Physics and Mathematical Sciences, Hangzhou Institute for Advanced Study, UCAS, Hangzhou 310024, China*
[4]*International Centre for Theoretical Physics Asia-Pacific, Beijing\|Hangzhou, China*
[5]*Key Laboratory for Research in Galaxies and Cosmology, Shanghai Astronomical Observatory, Shanghai 200030, China*

(Received 11 January 2021; accepted 15 February 2021; published 12 March 2021)

Two polarizations of the gravitational waves, the plus and cross modes, are derived from general relativity. However, alternative theories of gravity can yield the gravitational waves with up to six polarizations. Searching for the polarizations beyond plus and cross is an important test of general relativity. In principle, one spaceborne detector, like LISA, could measure the gravitational wave polarizations from a long time observation with its orbital motion. With comparable sensitivities, the joint LISA and TAIJI missions will improve the observations on the polarization predictions of theories beyond general relativity. In this work, a class of parametrized post-Einsteinian waveforms is employed to describe the alternative polarizations, and six parametrized post-Einsteinian parameters quantifying the deviation from the general relativity waveforms are examined by using the LISA-TAIJI network. Our results show that the measurements on amplitudes of alternative polarizations from joint LISA-TAIJI observation could be improved by more than 10 times compared to LISA single mission in an optimal scenario.

DOI: 10.1103/PhysRevD.103.064021

I. INTRODUCTION

From O1 to O3a of the Advanced LIGO and Virgo runs, about 50 gravitational wave (GW) events have been reported [1,2]. The mergers of binary compact objects offer the unique chance to test general relativity (GR) in the extra strong and dynamical gravitational field [3–5]. During these tests, the polarization of GWs is an important issue. General relativity (GR) predicts only two tensor polarizations: plus (+) and cross (×) modes. However, the metric theories of gravity may yield up to six polarizations, which are two vector modes, two scalar modes, and the two transverse-traceless polarization modes in GR. For example, scalar-tensor theories like as Brans-Dicke theory predict an extra scalar polarization (breathing, b) mode [6,7]; vector-tensor theories can excite vector modes (x, y modes) [8]; the Einstein-Aether theory [9] predicts the existence of five polarization modes; and tensor-vector-scalar theories such as TeVeS [10], bimetric [11,12], and stratified theories, such as the Lightman-Lee theory [13], predict the existence of all six polarization modes (+, ×, x, y, b, L), where L mode means longitudinal and is another scalar polarization mode.

In general, for the transient GW signals, at least three detectors are required to constrain additional modes [14]. Four detectors are necessary to constrain the vector modes, and in order to fully disentangle the polarization content of a transient signal, at least five detectors are needed to break all degeneracies [5,14]. After the Advanced Virgo joined the GW observation network, the tensor polarizations have been tested to see if they are preferred over the other modes with GW170814 and GW170817 [15,16]. The KAGRA in Japan has begun operating and will improve the measurement of polarizations in the near future [17–21].

The spaceborne detectors, including LISA [22], TAIJI [23], and TianQin [24], are planed to been launched around the 2030s, targeting to detect the GW in the low frequency band. As a benefit of the periodical motions orbiting the Sun/Earth, the detectors can observe (long-lasting) GW signals at different positions and orientations. And then one single mission, like LISA, could measure the polarizations independently [25,26], especially for the sources at an optimal position and inclination. However, for the massive black hole binaries (MBHBs), the duration of the signal is about a few weeks and may not be enough to constrain the polarizations. The joint observation from the LISA-TAIJI network may improve the resolution of the measurements. With the comparable sensitivities of the two missions, there will be lots of merits by LISA-TAIJI joint observations.

*Corresponding author.
wbhan@shao.ac.cn
†gwang@shao.ac.cn, gwanggw@gmail.com

Ruan *et al.* [27] and Wang *et al.* [28] demonstrated a significant improvement in sky localization capacities by the LISA-TAIJI network. Omiya and Seto [29] and Orlando *et al.* [30] calculated the overlap reduction functions of the two missions and evaluated the impacts of the joint observations on the stochastic GW observation. Liu *et al.* [31] estimated the constraint on polarizations from single TAIJI observations.

In this paper, following our previous work in [28], by using the LISA-TAIJI network, we evaluate the capacity of observation for the polarization predictions beyond general relativity. A set of parametrized post-Einsteinian (ppE) waveforms is employed to represent the GW signals of six potential polarization, and six ppE parameters are used to quantify the deviations of GW from GR. The Fisher information matrix algorithm is utilized to determine measurements on the six parameters from two MBHB sources. The results show that the measurements on the amplitudes of alternative polarizations from a joint LISA-TAIJI observation could be improved by more than tenfold compared to a LISA single mission in an optimal scenario.

This paper is organized as follows. In Sec. II, we introduce the model independent waveforms with GW and alternative polarization modes. In Sec. III, we specify the responding functions of the time-delay interferometry (TDI) to the polarizations and evaluate the average sensitivities for the different polarization modes. The Fisher information matrix method utilized and the determinations on the ppE parameters are presented in Sec. IV. We recapitulate our conclusions in Sec. V. (We set $G = c = 1$ in this work.)

II. PARAMETRIZED POST-EINSTEIN WAVEFORMS WITH ALL POLARIZATIONS

The GWs derived from GR have only two polarization modes, h_+ and $h_\times$; the time-domain waveforms of a binary system inspiral with quadrupole approximation are

$$h_+ = -\frac{2\mu M}{Dr}\cos 2\Phi(1+\cos^2\iota), \tag{1}$$

$$h_\times = -\frac{4\mu M}{Dr}\sin 2\Phi\cos\iota, \tag{2}$$

where M the total mass, μ is the reduced mass $\frac{m_1 m_2}{m_1+m_2}$, r the separation of two bodies, Φ the orbital phase, D is the luminosity distance, and ι is the inclination angle of the source with respect to the light-of-sight. The response signal in a detector to the GW will be

$$h_{\rm GR}(t) = F_+ h_+ + F_\times h_\times, \tag{3}$$

where F_+ and $F_\times$ are the antenna pattern functions of the detector to the two polarizations. On the other side, the frequency evolution of a binary under post-Newtonian (PN) approximation is a classical solved problem [32,33], and the GW from GR in frequency domain could be approximated as [34]

$$\tilde{h}_{\rm GR}(f) = \left(\frac{5\pi}{96}\right)^{1/2} A_{\rm GR}\frac{\mathcal{M}^2}{D}(\pi\mathcal{M}f)^{-7/6}e^{-i\Psi_{\rm GR}}, \tag{4}$$

where $\mathcal{M}$ is the chirp mass of the binary $(m_1m_2)^{3/5}/(m_1+m_2)^{1/5}$ and $A_{\rm GR}$ is the responding amplitude of the polarization modes $(+,\times)$ from a detector,

$$A_{\rm GR} = -F_+(1+\cos^2\iota) - 2iF_\times\cos\iota. \tag{5}$$

In general, GW metric perturbations at a given space-time point can be expressed as

$$h_{ij}(t,\hat{\Omega}) = h_a(t)e^a_{ij}(\hat{\Omega}), \tag{6}$$

where $\hat{\Omega}$ is the sky direction of a GW source. In metric theories of gravity, there are up to six possible polarization modes because the polarization tensors $e^a_{ij}(\hat{\Omega})$ could have a maximum of six combinations, which are defined as

$$e^+_{ab} = \hat{e}_x\otimes\hat{e}_x - \hat{e}_y\otimes\hat{e}_y, \tag{7}$$

$$e^\times_{ab} = \hat{e}_x\otimes\hat{e}_y + \hat{e}_y\otimes\hat{e}_{\rm x}, \tag{8}$$

$$e^{\rm x}_{ab} = \hat{e}_x\otimes\hat{e}_z + \hat{e}_z\otimes\hat{e}_x, \tag{9}$$

$$e^{\rm y}_{ab} = \hat{e}_y\otimes\hat{e}_z + \hat{e}_z\otimes\hat{e}_y, \tag{10}$$

$$e^{\rm b}_{ab} = \hat{e}_x\otimes\hat{e}_x + \hat{e}_y\otimes\hat{e}_y, \tag{11}$$

$$e^{\rm L}_{ab} = \sqrt{2}\hat{e}_z\otimes\hat{e}_z, \tag{12}$$

where the set of orthonormal unit vectors $\{\hat{e}_x,\hat{e}_y,\hat{e}_z\}$ is GW basis; i.e., $\hat{e}_z = -\hat{\Omega}$ is a unit vector in the direction of propagation of the GW, and $\hat{e}_z = \hat{e}_x\times\hat{e}_y$. Then in Eq. (6), $a = +,\times,{\rm x},{\rm y},{\rm b},{\rm L}$ are the polarization indices that correspond to two tensor modes (h_+, $h_\times$), two vector modes ($h_{\rm x}$, $h_{\rm y}$), and two scalar modes (breathing $h_{\rm b}$ and longitudinal $h_{\rm L}$).

By assuming all six polarization modes exist, an observed GW signal in a detector can be written as

$$h(t) = F_+h_+ + F_\times h_\times + F_{\rm x}h_{\rm x} + F_{\rm y}h_{\rm y} + F_{\rm b}h_{\rm b} + F_{\rm L}h_{\rm L}. \tag{13}$$

Similar to Eq. (3), the $F_{\rm x}$, $F_{\rm y}$, $F_{\rm b}$, and $F_{\rm L}$ are the response functions of the detector to the extra polarization modes beyond the GR. However, $h_{\rm x}$, $h_{\rm y}$, $h_{\rm b}$, and $h_{\rm L}$ are the GW waveforms for the corresponding polarizations, and they are derived in different forms from various theories. Also, not all of the polarization modes appear in different theories. For instance, the Brans-Dicke theory (a scalar-tensor theory) only predicts one more mode, $h_{\rm b}$. Vector-tensor theories usually predict the existence of preferred directions and the excitation of vector modes $h_{\rm x}$, $h_{\rm y}$ [8]. Einstein-Aether theories will allow five polarization modes [9], while the tensor-vector-scalar theories, bimetric and stratified theories, allow all six polarization modes [10–13].

The above alternative gravity theories predict a different formalism for a certain extra polarization. One can refer to Ref. [14] for the time-domain waveforms with different coupling parameters for a few of these theories. For the testing of these polarization modes, it is not convenient to focus on just one special theory. Alternatively, a model-independent waveform model, which can include a set of parameters corresponding to various theories, should be more appropriate for tests of polarization.

Furthermore, for data analysis, frequency-domain waveforms are will be more convenient than the time-domain ones. And the waveforms in frequency domain have different formulas for different theories not only due to the time-domain waveforms but also due to varied radiation reactions. A general framework that can incorporate the possible alternative theories of gravity will be convenient to test the potential polarizations beyond the GR.

To test the GR in the post-Newtonian limits, the parametrized post-Newtonian (ppN) formalism was developed in the 1970s [35–37]. The ppN formalism provided a good approach on tests of the gravity theories in the Solar System, binary pulsars, motion of objects around supermassive black hole, and etc. [7]. To test the alternative theories of gravity beyond the GR, by adopting a similar strategy like the ppN, Yunes and Pretorius [38] developed a parametrized post-Einsteinian (ppE) formalism to incorporate the alternative theories beyond GR. Chatziioannou *et al.* [14] extended a model-independent framework to include the complete polarization content. The ppE approach provides a approach for testing GR through the GW observations.

The standard ppE waveform in frequency domain can be generally expressed as

$$\tilde{h}(f) = \tilde{h}_{\rm GR}(f)[1 + \alpha' u^{a'}]e^{i\beta' u^{b'}}, \tag{14}$$

where (α', a') are ppE parameters on the amplitude modification, and (β', b') are parameters on the phase correction. Here, we use the superscript $'$ to distinguish the following parameters α, β, and b, which have coefficient differences defined in [14]. $u = \pi\mathcal{M}f$ when the dominant GW mode is considered. The waveform will return to the PN waveform described in GR $\tilde{h}_{\rm GR}(f)$ when the ppE parameters go to zero.

When the full six possible polarization modes are considered, by taking the waveform from the harmonic $l = 2$, a model-independent ppE framework from [14] is described as

$$\begin{aligned}\tilde{h}_{\rm ppE}(f) = \tilde{h}_{\rm GR}(1 + c\beta u_2^{b+5})e^{2i\beta u_2^b} + [\alpha_{\rm b}F_{\rm b}\sin^2\iota \\ + \alpha_{\rm L}F_{\rm L}\sin^2\iota + \alpha_{\rm x}F_{\rm x}\sin 2\iota + \alpha_{\rm y}F_{\rm y}\sin\iota] \\ \times \frac{\mathcal{M}^2}{D}u_2^{-7/2}e^{-i\Psi^{(2)}_{\rm GR}}e^{2i\beta u_2^b},\end{aligned} \tag{15}$$

where $u_2 \equiv (\pi\mathcal{M}f)^{1/3}$ as defined in this case, β and b are the free ppE parameters, c is a coefficient decided by b. $\alpha_{\rm b}$, $\alpha_{\rm L}$, $\alpha_{\rm x}$, and $\alpha_{\rm y}$ are the parameters related to the breathing, longitudinal, and vector polarization x and y modes, respectively. $F_{\rm b,L,x,y}$ are the response functions of one GW detector to each corresponding polarization mode. c is defined as follows to incorporate the conservative and dissipative corrections as defined by Eq. (11) in the Erratum [39] of [14],

$$c = -\frac{16}{15}\frac{b(3-b)(b^2+7b+4)}{b^2+8b+9}. \tag{16}$$

The relation between b and c means that the modification on the GW phase will definitely influence the amplitude as analyzed in [14]. The GW approximation in this work is based on the Eq. (15), and the antenna pattern functions for the polarization mode p. $F_{\rm p}$ for LISA-like detectors will be specified in the next section.

III. GW RESPONSE IN TDI

A. The LISA and TAIJI orbital configuration

The updated LISA mission proposed a 2.5×10^6 km arm length and trails the Earch by around 20° [22]. The formation plane of the three S/C would have a 60° inclination angle with respect to the ecliptic plane as shown in Fig. 1. The TAIJI mission proposed a LISA-like formation with a 3×10^6 km arm length [23]. The triangle constellation will be in front of the Earth by around 20°, as shown in Fig. 1.

With a separation of $\sim 1 \times 10^8$ km, the joint LISA-TAIJI observation from the long baseline will bring merits for GW detections. In our previous work [28], we evaluated the sky localization improvement of the joint observation on the supermassive black hole binaries. By employing the numerical mission orbit in [28,40], we will explore the detectability of the joint network to the alternative GW polarization modes beyond the GR.

B. Michelson and optimal TDI channels

The optimal channels of the first-generation Michelson TDI channel are employed to perform the detectability of

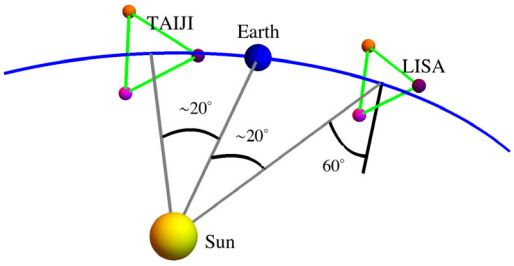

FIG. 1. The diagram of LISA and TAIJI mission orbital configurations.

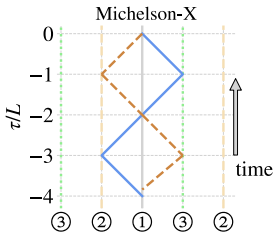

FIG. 2. The S/C layout-time delay diagrams for Michelson X channels as generated in [41].

the LISA/TAIJI mission. The Michelson X channel spacecraft (S/C) layout-time delay diagram is shown in Fig. 2, as generated in [41]. Following the diagram, the expression of measurements in the X channel will be [42].

$$\begin{aligned} \mathrm{X} = & [\mathcal{D}_{31}\mathcal{D}_{13}\mathcal{D}_{21}\eta_{12} + \mathcal{D}_{31}\mathcal{D}_{13}\eta_{21} + \mathcal{D}_{31}\eta_{13} + \eta_{31}] \\ & - [\eta_{21} + \mathcal{D}_{21}\eta_{12} + \mathcal{D}_{21}\mathcal{D}_{12}\eta_{31} + \mathcal{D}_{21}\mathcal{D}_{12}\mathcal{D}_{31}\eta_{13}], \end{aligned} \tag{17}$$

where $\mathcal{D}_{ij}$ is a time-delay operator, $\mathcal{D}_{ij}\eta(t) = \eta(t - L_{ij})$. The η_{ji} are the combined observables from S/Cj to S/Ci, which are defined as [43–45], and the specific expressions for this work are defined by Eq. (2) in [41].

A group of optimal TDI channels (A, E, and T) can be generated from linear combinations of the three Michelson channels (X, Y, and Z) as following [46,47]:

$$\mathrm{A} = \frac{\mathrm{Z} - \mathrm{X}}{\sqrt{2}}, \qquad \mathrm{E} = \frac{\mathrm{X} - 2\mathrm{Y} + \mathrm{Z}}{\sqrt{6}}, \qquad \mathrm{T} = \frac{\mathrm{X} + \mathrm{Y} + \mathrm{Z}}{\sqrt{3}}. \tag{18}$$

The Y and Z channels are obtained from cyclical permutation of the S/C indexes. The joint three optimal channels would represent the ultimate detectability of a LISA-like space mission. Therefore, the joint optimal channels are employed to study the capability of the LISA and TAIJI mission to the GW signals.

C. Response formulation of TDI channel

The final GW response of a TDI channel is combined from the response in each single link. The response to a GW + and × polarizations in a single link Doppler measurement has been formulated in [48,49], and specific formulas were described in Vallisneri and Galley [42] and Vallisneri *et al.* [47]. Tinto and da Silva Alves [50] developed the response functions for the alternative polarizations and evaluated the sensitivities. We employ the formulas as follows to investigate the response of TDI to the six polarizations.

For a GW source locating at ecliptic longitude λ and latitude θ with respect to the Solar System barycentric coordinates, the GW propagation vector will be

$$\hat{k} = -(\cos\lambda\cos\theta, \sin\lambda\cos\theta, \sin\theta). \tag{19}$$

The + or × polarization tensors of the GW signal, as well as the (potential) alternative polarization tensor, scalar breathing (b), scalar longitudinal (L), vector x and y, combining with the factors from inclination angle ι of the source are

$$\begin{aligned} \mathrm{e}_{+} &\equiv \mathcal{O}_1 \cdot \begin{pmatrix} 1 & 0 & 0 \\ 0 & -1 & 0 \\ 0 & 0 & 0 \end{pmatrix} \cdot \mathcal{O}_1^T \times \frac{1+\cos^2\iota}{2}, \qquad \mathrm{e}_{\times} \equiv \mathcal{O}_1 \cdot \begin{pmatrix} 0 & 1 & 0 \\ 1 & 0 & 0 \\ 0 & 0 & 0 \end{pmatrix} \cdot \mathcal{O}_1^T \times i(-\cos\iota), \\ \mathrm{e}_{\mathrm{b}} &\equiv \mathcal{O}_1 \cdot \begin{pmatrix} 1 & 0 & 0 \\ 0 & 1 & 0 \\ 0 & 0 & 0 \end{pmatrix} \cdot \mathcal{O}_1^T \times \sin^2\iota, \qquad \mathrm{e}_{\mathrm{L}} \equiv \mathcal{O}_1 \cdot \begin{pmatrix} 0 & 0 & 0 \\ 0 & 0 & 0 \\ 0 & 0 & 1 \end{pmatrix} \cdot \mathcal{O}_1^T \times \sin^2\iota, \\ \mathrm{e}_{\mathrm{x}} &\equiv \mathcal{O}_1 \cdot \begin{pmatrix} 0 & 0 & 1 \\ 0 & 0 & 0 \\ 1 & 0 & 0 \end{pmatrix} \cdot \mathcal{O}_1^T \times \sin\iota\cos\iota, \qquad \mathrm{e}_{\mathrm{y}} \equiv \mathcal{O}_1 \cdot \begin{pmatrix} 0 & 0 & 0 \\ 0 & 0 & 1 \\ 0 & 1 & 0 \end{pmatrix} \cdot \mathcal{O}_1^T \times i\sin\iota, \end{aligned} \tag{20}$$

with

$$\mathcal{O}_1 = \begin{pmatrix} \sin\lambda\cos\psi - \cos\lambda\sin\theta\sin\psi & -\sin\lambda\sin\psi - \cos\lambda\sin\theta\cos\psi & -\cos\lambda\cos\theta \\ -\cos\lambda\cos\psi - \sin\lambda\sin\theta\sin\psi & \cos\lambda\sin\psi - \sin\lambda\sin\theta\cos\psi & -\sin\lambda\cos\theta \\ \cos\theta\sin\psi & \cos\theta\cos\psi & -\sin\theta \end{pmatrix}, \tag{21}$$

where ψ is the polarization angle. The response to the GW polarization p in the link from S/Ci to j will be

$$y^h_{\mathrm{p},ij}(f) = \frac{\hat{n}_{ij}\cdot \mathrm{e}_{\mathrm{p}}\cdot\hat{n}_{ij}}{2(1-\hat{n}_{ij}\cdot\hat{k})} \times [\exp(2\pi i f(L_{ij} + \hat{k}\cdot p_i)) - \exp(2\pi i f\hat{k}\cdot p_j)], \tag{22}$$

where $\hat{n}_{ij}$ is the unit vector from S/Ci to j, L_{ij} is the arm length from S/Ci to j, and p_i is the position of the S/Ci in the Solar System barycentric (SSB) ecliptic coordinates.

The response of a TDI combination for a specific polarization p in the frequency domain will be simplified by summing up the responses in the time shift single links. For instance, the response in the X channel could be described by

$$\begin{aligned} F_{\mathrm{X,p}}(f) = &(-\Delta_{21} + \Delta_{21}\Delta_{13}\Delta_{31})y^h_{\mathrm{p},12} \\ &+ (-1 + \Delta_{13}\Delta_{31})y^h_{\mathrm{p},21} \\ &+ (\Delta_{31} - \Delta_{31}\Delta_{12}\Delta_{21})y^h_{\mathrm{p},13} \\ &+ (1 - \Delta_{12}\Delta_{21})y^h_{\mathrm{p},31}, \end{aligned} \tag{23}$$

where $\Delta_{ij} = \exp(2\pi i f L_{ij})$. The GW responses in the optimal A, E, and T channels are obtained by applying Eq. (18) straightforwardly. One polarization of the GW waveform in a TDI channel could be expressed as $\tilde{h}_{\mathrm{TDI,p}} = F_{\mathrm{TDI,p}}\tilde{h}$ as will be shown in Fig. 4, where the $\tilde{h}$ is the *intrinsic* GW waveform in the frequency domain. By using Eq. (15), the alternative GW waveform with six polarizations in one TDI channels could be modified as [14]

$$\begin{aligned} \tilde{h}_{\mathrm{ppE,TDI}}(f) = &[(F_+ + F_\times)(1 + c\beta u_2^{b+5}) + \alpha_{\mathrm{b}}F_{\mathrm{b}} + \alpha_{\mathrm{L}}F_{\mathrm{L}} \\ &+\alpha_{\mathrm{x}}F_{\mathrm{x}} + \alpha_{\mathrm{y}}F_{\mathrm{y}}]\tilde{h}_{\mathrm{GR}}e^{2i\beta u_2^b}, \end{aligned} \tag{24}$$

where $\tilde{h}_{\mathrm{GR}}$ is the intrinsic GW waveform from GR described by the approximant IMRPhenomPv2 [51] in our calculations. The β, b, α_{b}, α_{L}, α_{x}, and α_{y} are the six ppE parameters to be determined.

D. The average sensitivities of LISA to the polarizations

Considering the various response in TDI channels, we evaluate the average sensitivities of the LISA and LISA-TAIJI network to the six polarization modes at first. Following the method we used in Wang *et al.* [41], 10^5 sources are simulated randomly, which are located over the sky and polarization at each frequency. The response of one TDI channel to a polarization mode is calculated by using the Eqs. (18)–(23) with an optimal inclination (for instance, inclination $\iota = 0$ yields the maximum amplitude for tensor polarization, and $\iota = \pi/2$ yields the strongest GW for scalar polarizations). The median responses of joint A+E+T channels over sky and polarization angle are chosen to represent the average capacity of one mission to a specific GW polarization mode. And the response of LISA and TAIJI to a source are calculated simultaneously.

The acceleration noise and optical path noise are considered to evaluate the sensitivity of LISA/TAIJI. The noise budgets are from the updated upper limit of their noise requirements [22,52]. The acceleration noise S_{acc} requirements are assumed to be the same for both LISA and TAIJI,

$$S_{\mathrm{acc}}^{1/2} = 3\times10^{-15}\frac{\mathrm{m/s^2}}{\sqrt{\mathrm{Hz}}}\sqrt{1+\left(\frac{0.4\,\mathrm{mHz}}{f}\right)^2}\sqrt{1+\left(\frac{f}{8\,\mathrm{mHz}}\right)^4}. \tag{25}$$

And the optical path noises S_{op} requirement for two missions are slightly different, which are

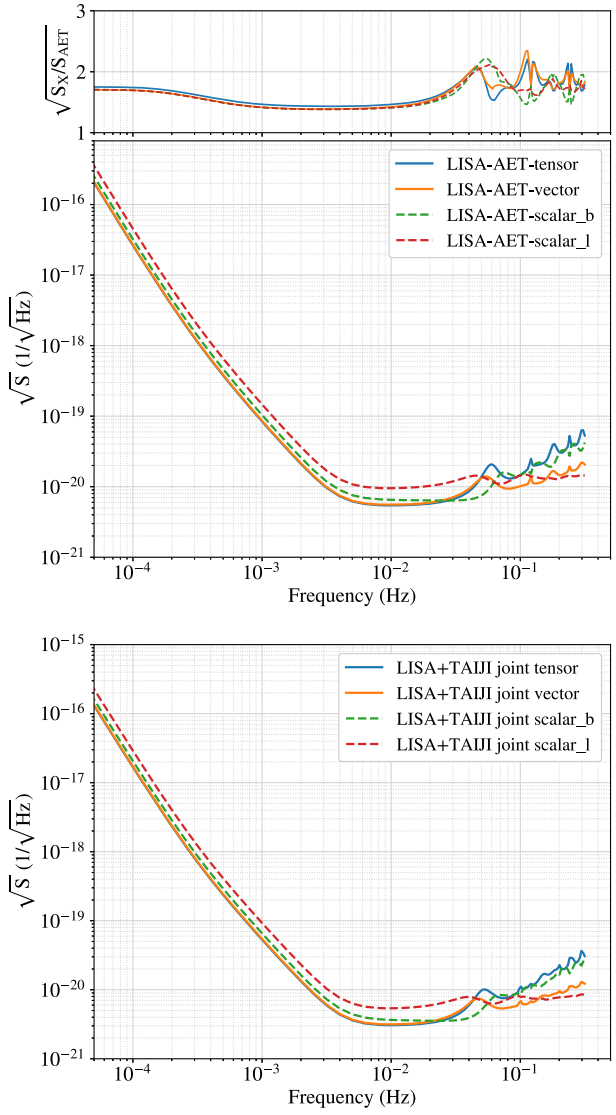

FIG. 3. The average sensitivities of LISA mission (upper panel) and joint LISA-TAIJI network (lower panel) to the different polarization modes at the optimal inclination angles. The upper plot of the upper panel shows the joint LISA A + E + T channel would improve the sensitivity by a factor of $\sqrt{2}$ to 2 compared to its fiducial Michelson X channel. The lower panel shows the joint LISA-TAIJI network can improve the sensitivities by a factor of $\geq\sqrt{2}$ than the single LISA mission.

$$S_{\mathrm{op,LISA}}^{1/2} = 10 \times 10^{-12} \frac{\mathrm{m}}{\sqrt{\mathrm{Hz}}} \sqrt{1 + \left(\frac{2\,\mathrm{mHz}}{f}\right)^4},$$
$$S_{\mathrm{op,TAIJI}}^{1/2} = 8 \times 10^{-12} \frac{\mathrm{m}}{\sqrt{\mathrm{Hz}}} \sqrt{1 + \left(\frac{2\,\mathrm{mHz}}{f}\right)^4}. \quad (26)$$

The combined noise PSDs of the TDI channels are calculated by implementing the algorithm in [41,53].

The average sensitivities of the LISA's A + E + T channel and joint LISA-TAIJI network to a polarization mode p are obtained by

$$\mathrm{S}_{\mathrm{LISA,p}} = \left(\sum_{\mathrm{A,E,T}} \frac{|F_{\mathrm{TDI,p}}|^2}{\mathrm{S}_{n,\mathrm{TDI}}} \right)^{-1}, \quad (27)$$

$$\mathrm{S}_{\mathrm{joint,p}} = \left(\sum_{\mathrm{LISA}}^{\mathrm{TAIJI}} \sum_{\mathrm{A,E,T}} \frac{|F_{\mathrm{TDI,p}}|^2}{\mathrm{S}_{n,\mathrm{TDI}}} \right)^{-1}. \quad (28)$$

The average sensitivities of the LISA mission for different polarization modes are shown in the upper panel of Fig. 3. The upper plot of the upper panel shows the increase of joint A + E + T sensitivity compared to the fiducial Michelson X channel. As we expatiated in Wang *et al.* [53], the joint A + E + T channels will improve the sensitivity by a factor of $\sqrt{2}$ to 2 times than the X single channel. The joint LISA-TAIJI observation can further improve the sensitivity of LISA by a factor of $\geq \sqrt{2}$ as shown in the lower panel of Fig. 3. We can also notice that the sensitivity for the vector mode and the longitudinal mode do not quickly decline as the tensor mode, and this should be due to the higher response at the high frequency band in the TDI for these polarization modes as discussed in [50,54].

The sensitivities for alternative polarizations in Fig. 3 are calculated by assuming the ppE parameter $\alpha_i = 1$ in Eq. (24) and an optimal inclination ι in Eq. (20). The sensitivities could be scaled by the tuned factors.

IV. CONSTRAINING PPE PARAMETERS FROM SMBH BINARY COALESCENCE

A. Source selections

Following our previous work [28], we choose the supermassive black hole (SMBH) binaries with a mass ratio $q = 1/3$ at redshift $z = 2$ to examine the detectability of the LISA-TAIJI network and compare the results to a single LISA mission. Two masses setups are employed which are source1 ($m_1 = 10^5\ M_\odot$, $m_2 = 3.3 \times 10^4\ M_\odot$) and source2 ($m_1 = 10^6\ M_\odot$, $m_2 = 3.3 \times 10^5\ M_\odot$). Another motivation for this selection is that these two sources could be well sky localized by the two detector network as studied in [28]. Therefore, an optimistic scenario would be assumed that the source location (direction and distance) could be determined by a multi-messenger observation, and the known source location may improve the achieved results.

The redshifted GW amplitudes of two sources in the selected TDI channels and the ASDs of the channels are shown in Fig. 4. The amplitudes incorporate the response function of the TDI channels $2\sqrt{f}|\tilde{h}_{\mathrm{GR}} * F_{\mathrm{TDI,p}}|$ for the specific source parameters ($\theta = \pi/10, \iota = 0.55$ rad, $\psi = \pi/3$) through the frequency band in the last one year of coalescing. The ASDs of the TDI channels are the noise level from the acceleration and optical-path noises. The ASDs of A and E channels are identical, while the amplitudes of GW signals in their channels are different. The frequencies at 30 days before the coalescences are annotated in the plot, and the SNRs from the last 30 days are expected to be dominant for the detections. As we previously studied in [41,53], the location around the ecliptic latitude $\theta = 18°$ would be an optimal choice for the average response, and the longitude of sources is coordinated with the positions of the LISA and TAIJI to have an optimal response. The inclination of the sources is one of the key factors which relates to the cadence of the different polarization amplitudes. By presuming the polarization modes beyond GR are much less significant than +/× polarizations from GW, the inclination angle is set to be $\iota = 0.55$ rad, which is close to the favored angle of the detections as shown in the upper plot of Fig. 6 [55]. And we will also perform the investigations varying the inclination in Sec. IV D. The polarization angle is set to be $\psi = \pi/3$.

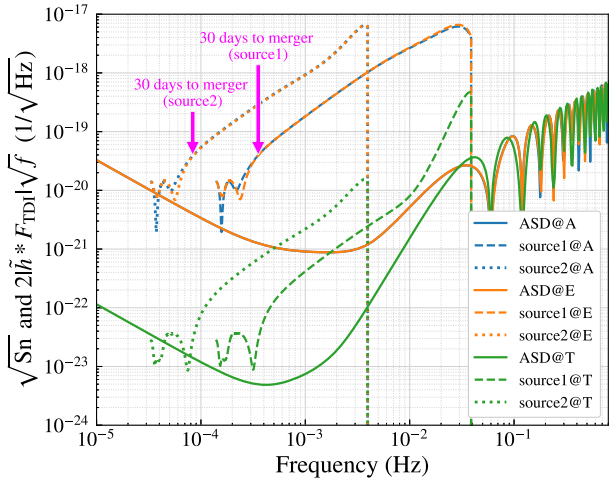

FIG. 4. The redshifted GW amplitudes $2\sqrt{f}|\tilde{h}_{\mathrm{GR}} * F_{\mathrm{TDI,p}}|$ of the selected sources and ASDs in the optimal TDI channels for one year evolution before coalescence. The GW amplitudes include the TDI response function $F_{\mathrm{TDI,p}}$ for the sources with geometric angles ($\theta = \pi/10, \iota = 0.55$ rad, $\psi = \pi/3$). The ASDs of the TDI noises include the acceleration noises and optical path noises. The source1@TDI indicates GW amplitude of the source1 ($m_1 = 10^5\ M_\odot$, $q = 1/3$, $z = 2$) in the TDI channels, and source2@TDI indicates the source2 ($m_1 = 10^6\ M_\odot$, $q = 1/3$, $z = 2$).

For the source1 ($m_1 = 10^5\ M_\odot$, $q = 1/3$), the GW frequency evolution during the one year to merger will change from 0.14 mHz to 40 mHz, and the corresponding $u_2^3 = \pi\mathcal{M}f$ value changes from [0.0003, 0.09]. And the GW frequency from the binary ($m_1 = 10^6\ M_\odot$, $q = 1/3$) will start from 0.033 mHz to 4 mHz, and the range of u_2^3 is [0.00075, 0.09]. As estimated in Cornish *et al.* [56], the bounds limits of β at a given b is expected to be inversely proportional to the SNR and the range of u_2^b.

B. Antenna patterns for polarizations

The response of a GW interferometer to the GW signals changes with the source locations and orientations. The antenna patterns of a ground-based interferometer for the alternative GW polarization modes have been plotted in [25,26]. To illustrate the antenna pattern of a LISA-like mission, the joint responses of the A, E, and T TDI channels to each polarization in the detector frame are shown in Fig. 9 in the Appendix. As Fig. 9 shows, the most sensitive directions for the tensor modes are the normal/polar directions with respect to the interferometer plane, while the most sensitive directions for the scalar and vector x polarization are the equatorial directions. The optimal direction for the vector y polarization observation is the direction $\pi/4$ with respect to the formation plane.

As aforementioned, the S/C formation plane of a LISA-like mission has a 60° inclination angle with respect to the ecliptic plane. Considering the detector's orbital motion, the SSB coordinates are employed to incorporate the modulations with the relative positions and orientation changes between the interferometer and the GW sources. The instantaneous sensitivities of LISA for the different polarization modes are shown in Fig. 5. The sensitivity is calculated by using Eq. (27) at 10 mHz for the $\psi = \pi/3$ and optimal inclinations ι for each polarization mode. As we can see in two plots of the upper panel, the most sensitive direction for the tensor modes observation is around ±30° ecliptic latitude facing by the S/C triangular formation. For scalar polarization modes, the most sensitive directions of the tensor modes are the most insensitive directions. For vector modes, besides the insensitive directions to the normal directions of the S/C formation plane, there are some other unresponsive directions. This antenna pattern also will change with the geometric angles (ψ and ι), the GW frequency, and the time. With a 40° separation from LISA as shown in Fig. 1, the TAIJI mission is expected to have a similar antenna pattern with ∼40° spatial shifted along the ecliptic latitude. The joint LISA and TAIJI

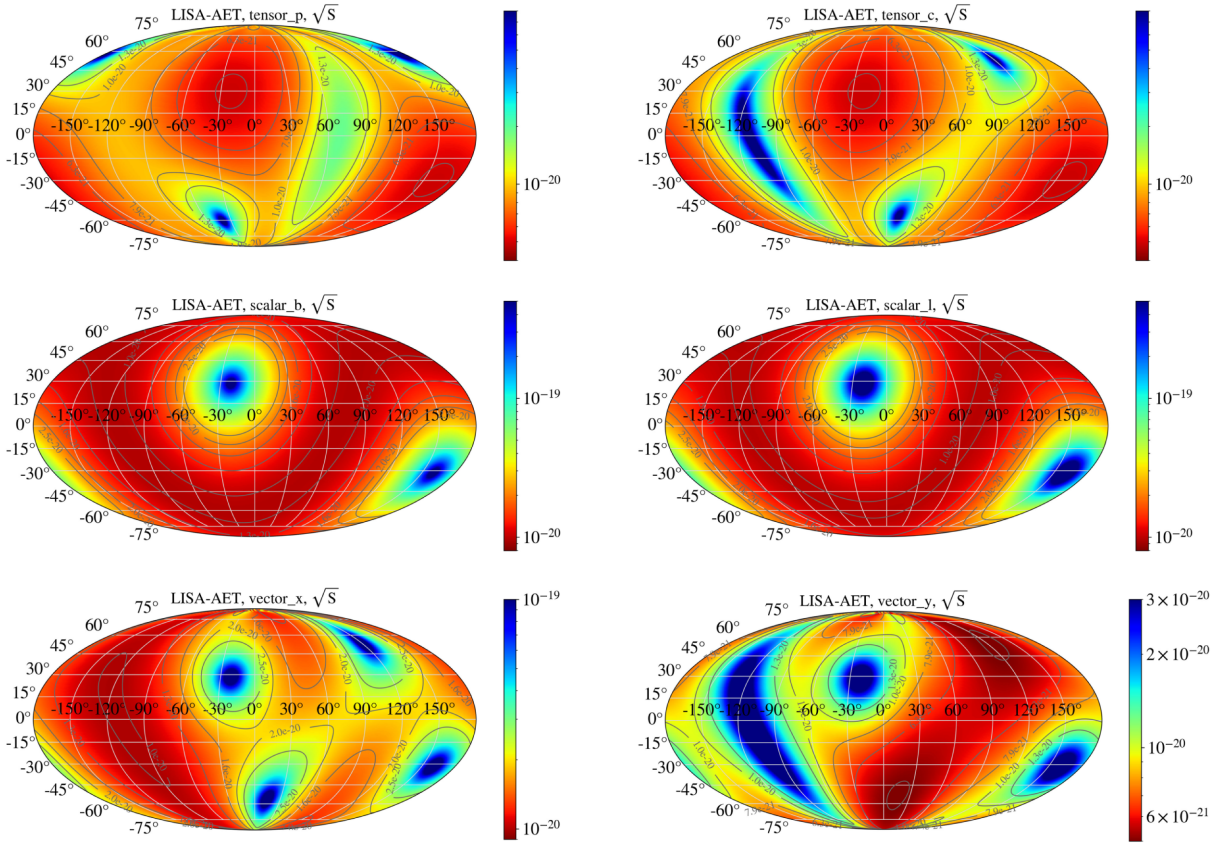

FIG. 5. The instantaneous sensitivities of LISA joint A + E + T channels for various polarization modes at 10 mHz. The ψ is set to be $\pi/3$, and inclination ι is optimal for each polarizations.

network will improve their sky coverage and enhance their detectability as we will see in the following subsections.

In this work, the coalescing SMBH binaries are selected to investigate the polarization observations, and the GW signals observations are mainly concentrated in the last one month as indicated in Fig. 4. On the other side, the observations of dominant tensor polarizations have the inverse favored sky direction against other alternative polarizations. It would be a trade-off for the selections of the source location and merger time. When the observation simulation is beneficial to the tensor modes, the SNR could increase and ppE parameters β and b could be well constrained. Other polarization modes could be poorly observed and parameters α_i may be underestimated and vice versa. In this investigation, the sources are selected to make their mergers happen around detectors' sensitive directions for the tensor mode.

C. Fisher information method

The Fisher information matrix (FIM) is applied in this investigation to determine the uncertainty of the parameter estimation from the GW observation as used in [[28,57–60] and references therein]. The FIM from the single LISA mission is obtained by summing up the three optimal channels (A, E, and T), and the joint FIM of the LISA-TAIJI network is achieved by summing up the FIM from each mission,

$$\Gamma_{ij} = \sum_{\text{LISA}}^{\text{TAIJI}} \sum_{\text{A,E,T}} \left(\frac{\partial \tilde{h}_{\text{ppE,TDI}}}{\partial \xi_i} \middle| \frac{\partial \tilde{h}_{\text{ppE,TDI}}}{\partial \xi_j} \right), \tag{29}$$

with

$$(g|h)_{\text{TDI}} = 4\text{Re} \int_0^\infty \frac{g^*(f)h(f)}{S_{\text{TDI}}(f)} \mathrm{d}f, \tag{30}$$

where $\tilde{h}_{\text{ppE,TDI}}$ is the frequency domain GW waveform with all polarization modes as described by Eq. (24), ξ_i is the ith parameter to the determined, and $S_{\text{TDI}}(f)$ is the noise PSD of one TDI channel from LISA or TAIJI.

In this investigation, 15 parameters are considered to describe the GW signal of a binary binary inspiral, which are ecliptic longitude and latitude (λ, θ), polarization angle ψ, inclination ι, luminosity distance D, the coalescence time and phase (t_c, ϕ_c), the total mass of binary M and mass ratio q, and the six ppE parameters $(\beta, b, \alpha_{\text{b}}, \alpha_{\text{L}}, \alpha_{\text{x}}, \alpha_{\text{x}})$. Two scenarios are considered to implement the FIM calculations. The first one is that the location of the source is unknown and the FIM is calculated for full 15 parameters. The second case is that the location of GW source is known from other associated observation, and the FIM is calculated for 12 parameters, excluding the three parameters (λ, θ, D).

The variance-covariance matrix of the parameters could be obtained by

$$\langle \Delta\xi_i \Delta\xi_j \rangle = (\Gamma^{-1})_{ij} + \mathcal{O}(\rho^{-1}). \tag{31}$$

The standard deviations σ_i and correlation coefficients σ_{ij} of the parameters for the high SNR $\rho \gg 1$ will be

$$\sigma_i \simeq \sqrt{(\Gamma^{-1})_{ii}},$$
$$\sigma_{ij} = \frac{\text{cov}(\xi_i, \xi_j)}{\sigma_i \sigma_j} \simeq \frac{(\Gamma^{-1})_{ij}}{\sigma_i \sigma_j}. \tag{32}$$

We focus on the ppE parameters determinations from LISA and the improvements from LISA-TAIJI joint observations in this work.

D. Results with varying inclination

We examine the detectability of the ppE parameter varying with the inclination of sources in this subsection. The amplitude of a GW signal is modulated with the inclination ι of the binary as read from Eq. (20). With only considering the two GW polarizations from GR, the distribution of inclination ι from the detections is expected to be [55]

$$p_{\text{tensor}}(\iota) \propto (1 + 6\cos^2\iota + \cos^4\iota)^{3/2} \sin\iota. \tag{33}$$

The normalized distribution is shown by the blue curve in the upper plot of Fig. 6. Similarly, if the vector polarizations or the scalar polarization is only considered, the corresponding distributions of inclination angle will be

$$p_{\text{vector}}(\iota) \propto (\sin^2\iota\cos^2\iota + \sin^2\iota)^{3/2} \sin\iota,$$
$$p_{\text{scalar}}(\iota) \propto \sin^7\iota. \tag{34}$$

Their curves are shown in Fig. 6 upper plot by the orange and green curves, respectively. These distributions show the favored inclinations by the different polarizations, the most favored inclination by the tensor polarization is around $\iota = 0.55$ rad, and the distributions of ι have the peaks around $\pi/2 = 1.57$ for both vector and scalar polarizations.

By assuming the $\alpha_i = 1$ for the alternative polarizations and tensor polarizations from GR, their SNRs varying with the inclinations from the two selected sources are shown in the lower plot of Fig. 6. The SNR from ($\iota = \pi/2$, edge-on) will be $1/\sqrt{8}$ of SNR from ($\iota = 0/\pi$, face-on/off) for the dominant tensor mode. For the inclination selection, considering the symmetry effects of the inclination in $[0, \pi/2]$ and $[\pi/2, \pi]$ range, we perform the investigations for $\iota = n\pi/24 (n = 1 \text{ to } 11)$. One reason to avoid the $\iota = 0$ is the astrophysical unlikely as shown in the upper plot of Fig. 6; another reason is that $\iota = 0$ or $\pi/2$ will dissolve some polarizations and make the FIM singular. The ppE parameter b is given different values for the different gravitational theories as shown in Table I of [56]. For the first step, we pick the $b = -3$, which corresponds to the massive graviton theory [61–67], and we investigate the other b valves in the next step. The β parameter is roughly

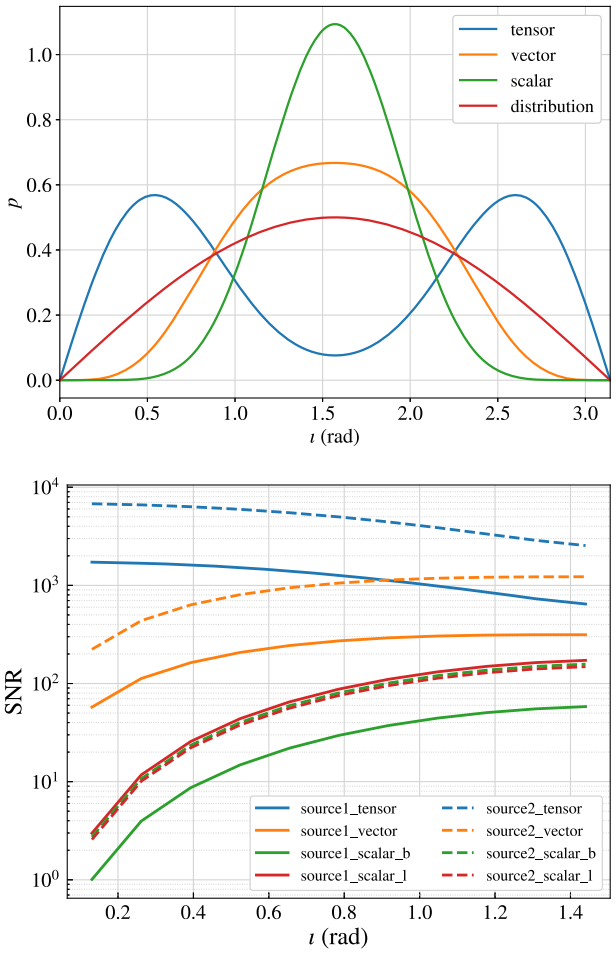

FIG. 6. The distributions of the inclination ι from expected detections considering the solo tensor, vector, and scalar polarization modes (upper panel) and the LISA's SNR of polarizations for corresponding $\alpha_i = 1$ from two selected sources with the inclinations (lower panel). The *tensor* curve shows the distribution of ι from the standard GR GW detections which are described by Eq. (33) [55]. The *vector* and *scalar* curve show the distributions of ι when the solo vector or scalar polarization GW waveform is detected as described by Eq. (34). The *distribution* curve shows the distribution of ι from geometry, $p(\iota) \propto \sin\iota$.

set to be 0.01 from the bounded result at $b = -3$ in [56]. The six ppE parameters are fixed for the FIM calculations, which are $(\beta, b, \alpha_b, \alpha_L, \alpha_x, \alpha_y) = (0.01, -3, 0, 0, 0, 0)$.

The constraints on ppE parameters from the source1 $(m_1 = 10^5\ M_\odot, q = 1/3, z = 2)$ and source2 $(m_1 = 10^6\ M_\odot, q = 1/3, z = 2)$ observations for different inclination angles are shown in Fig. 7. The uncertainties of ppE parameters β and b get improved when the inclination approaches 0 (or π) as shown in the two plots in the upper panel. Comparing to the LISA single detector, the joint LISA-TAIJI observation can improve the accuracy of the determination by a factor of ∼2, which should be the contribution of a twofold SNR. When the position of sources are known and the location parameters (λ, θ, D) are excluded, it only slightly improves the constraints from the single LISA observation and does not show improvement for the LISA-TAIJI joint observation. Comparing the constraints from the two sources, the source1 shows a better ability to measure parameters β and b than the source2. This could be due to the source1 having a relatively larger frequency range in the one year evolution and then having a larger range of the u_2. The wider range of u_2 could improve measurements on the parameter β and b [56]. For the $\iota = 0.55$ rad, the uncertainty of β could be constrained by the source1 in 9×10^{-6} from the LISA observation, and it could be constrained in 5×10^{-6} by the joint observation. The uncertainty of the parameter b could be bound in 5×10^{-4} by LISA from source1 observation and be within 2.5×10^{-4} by the LISA-TAIJI network. In general, at any inclination case, the joint LISA-TAIJI observation could improve the β and b determinations by a factor of ∼2.

The measurement uncertainties of ppE α_i from the two sources are shown by the middle and lower plots in Fig. 7. For these four parameters, the joint LISA-TAIJI network presents significant advantages. Without knowing the position of the source, the joint observation could improve the parameter measurements by more than ∼10 times in most of the cases except the more than ∼4 times improvement for the α_b. For the α_b, α_L, and α_y, their uncertainties tend to decrease with the increase of the ι, and the α_x is better measured around the $\iota = \pi/4$. We infer these tendencies from Eq. (20) which shows that the amplitudes of scalar breathing, scalar longitudinal, and vector y polarization modes increase with the selected inclination angles, and the amplitude of vector x mode has the maximum at $\iota = \pi/4$.

Compared to the results from two sources, the uncertainties of parameters α_b and α_L from source2 are moderately worse than the results from source1 for all scenarios (the single LISA or joint observation, unknowing or knowing the sky location) as two plots shown in the middle panel. However, for the measurement on the α_x and α_y, the results from source1 observations from the single LISA mission are still better than the results from source2; the joint observations could promote the source2 to a better constraint than source1, which could, due to the TAIJI mission, observe the source2 with a better response than source1. For the inclination $\iota = 0.55$ rad, the joint LISA-TAIJI observation could improve the parameter accuracy by more than 10 times compared to a single LISA observation for α_L, α_x, and α_y; if the position of the source is known and excluded from FIM calculation, the uncertainties of parameters could further decrease, and this should be due to the degeneracy removed between the sky location and α_i.

E. Results with varying ppE parameters b and β

In this subsection, we examine the impact of the joint LISA-TAIJI observation on the measurements of ppE parameters with different given β and b values. As aforementioned, the inclination ι of a source tunes the

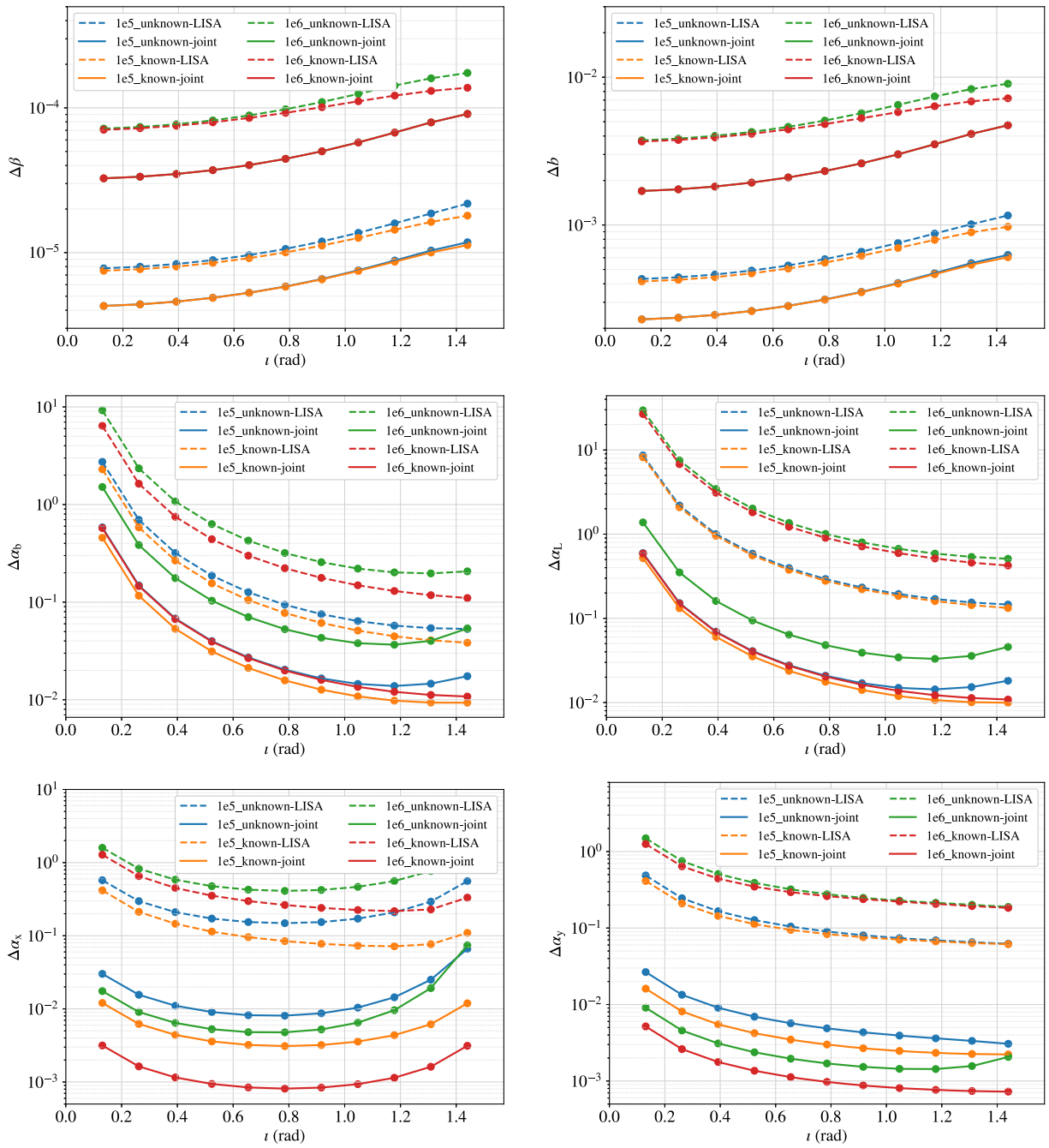

FIG. 7. The uncertainties of ppE parameters varying with the inclination ι from the source1 ($m_1 = 10^5\ M_\odot, q = 1/3, z = 2$) and source2 ($m_1 = 10^6\ M_\odot, q = 1/3, z = 2$ for ppE parameters setup $(\beta, b, \alpha_b, \alpha_L, \alpha_x, \alpha_y) = (0.01, -3, 0, 0, 0, 0)$. Four scenarios results are shown in each plots which are (1) the result from the single LISA observation without knowing the position of the source (m_1_unknown-LISA), (2) the result from joint LISA-TAIJI observation without information of source location (m_1_unknown-joint), (3) the result from the LISA observation with knowing position of the source and the FIM calculation excluding the three parameters: direction of the source (λ, θ), and distance of the sources D ($m1$_known-LISA), and (4) the result from LISA-TAIJI joint observation with knowing the position of the source (m_1_known-joint). In the two plots in the upper panel, the curves for 1e6_unkonwn-joint and 1e6_known-joint are overlapped.

amplitudes of each GW polarization and affects the SNR of the detection. Considering the tensor polarizations are dominant for the GW radiation from the coalescing compact binaries [4,16,20], we perform the investigations by choosing the fixed $\iota = 0.55$ rad. The four α_i coefficients on polarization amplitudes are set to be zero as the fiducial value ($\alpha_b = \alpha_L = \alpha_x = \alpha_x = 0$). Considering the parameter β has been bound at a given b from the PSR

J0737-3039 [68] and the LIGO and LISA simulation [56], our choices of β at a given b are shown by the purple triangles in the first plot of Fig. 8. And the FIM is calculated subsequently by settling each pair β and b.

The constraints on the ppE parameters with different β and b are shown in Fig. 8. The upper two plots show the results for β and b from the source1 $(m_1 = 10^5\ M_\odot, q = 1/3, z = 2)$ and source2 $(m_1 = 10^6\ M_\odot, q = 1/3, z = 2)$.

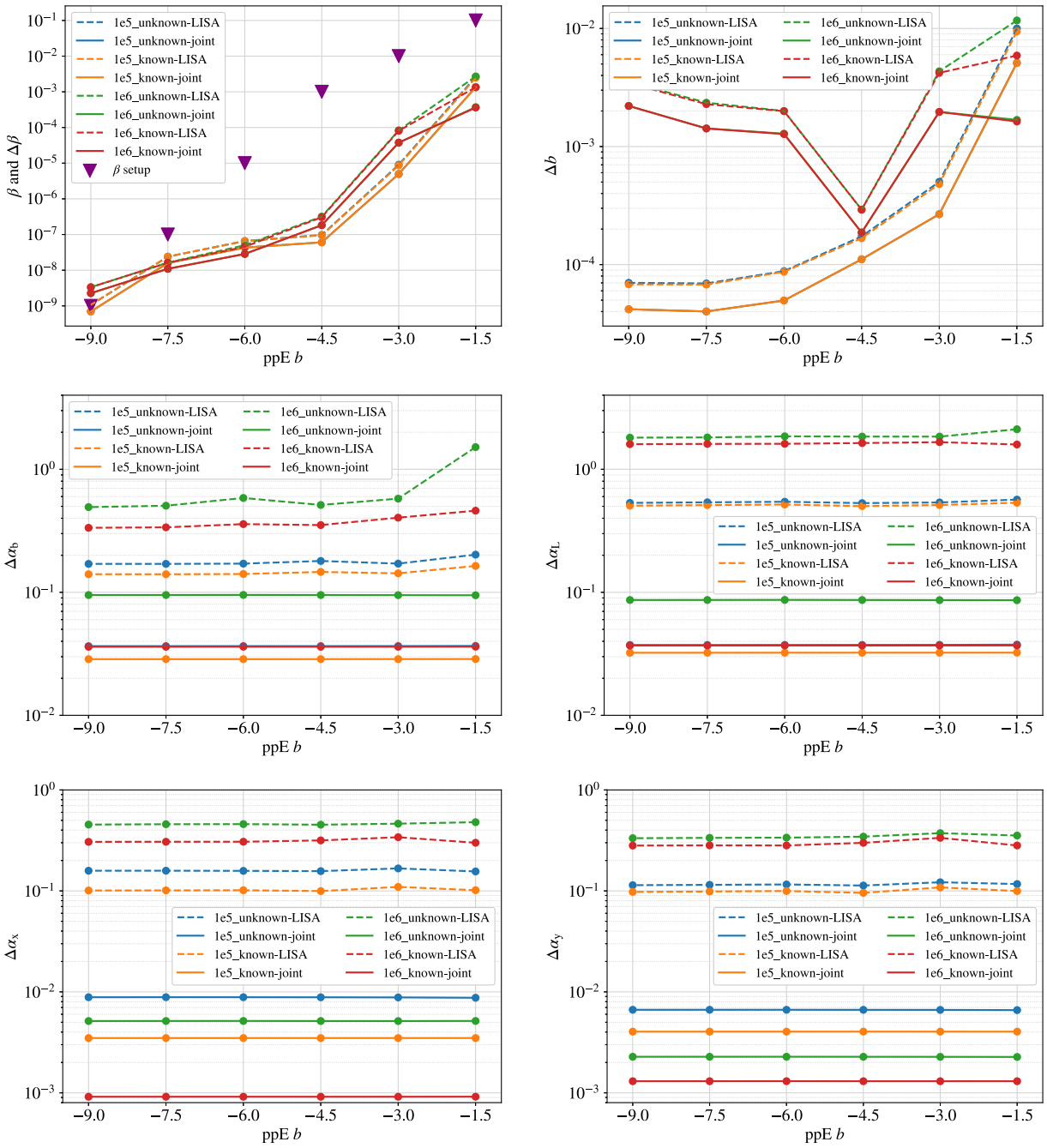

FIG. 8. The constraints of ppE parameters with different β and b from the LISA observation and LISA-TAIJI joint observations. The upper two plots show the results for β and b, and the middle and lower panels are the results for alternative coefficients α_i. The (purple) triangles are the β setups at a given b values which roughly referred from bounds in Cornish *et al.* [56]. The legend labels are same defined as in Fig. 7, the keyword with 1e5 or 1e6 indicates the respective source1 or source2, and a label with unknown/know shows if the position of source (λ, θ, D) is included/excluded in the FIM calculations. In the upper two plots, the unknown and known curves are overlapped for each scenarios. In the two plots in upper panel, the paired curves for m_1_unkonwn-joint and m_1_known-joint are overlapped.

As we can read from the upper left plots, for the presets of β and b, the constraints on β get better with the b decreases for both of the two selected sources. The source1 shows a relatively better determination of β by around one order than the source2 for the $(\beta = 10^{-2}, b = -3)$. For other cases, no significant difference between their results. The joint observation of the LISA-TAIJI network could improve by a factor of ~ 2 as shown more clearly in the previous subsection. For the measurement on parameter b, the source1 demonstrates more than 10 times a better constraint than source2 for $b < -4.5$. And the joint observation also can improve by a factor of ~ 2 on the parameter determination. The knowledge of the source position has a little improvement on the measurement since the sky location could be resolved from the loud signals, and their curves are overlapped with the unknown cases. The measurements of α_i are shown in the middle and lower panels. Considering the α_i are relatively independent of the β and b selections, the constraint on the α_i are almost have no change with the β and b values.

We conclude that, for the ppE parameter $(\beta, b, \alpha_{\rm b}, \alpha_{\rm L}, \alpha_{\rm x}, \alpha_{\rm y})$ measurements from the selected sources, compared to the LISA single detector observation, the joint observation of the LISA and TAIJI network could improve for the β and b measurement by a factor of ~ 2; the coefficients of alternative polarization modes α_i could be improved by more than ~ 10 times. With knowing the position of the source, all the accuracy of the polarization coefficients α_i could be further improved for some cases. For the significant promotions on the measurement of α_i, we ascribe the sky coverage compensation for LISA and TAIJI missions as inferred in Fig. 5. For our selected locations of the GW sources, the LISA could efficiently observe the GW tensor polarization modes and insensitively detect the other polarization modes. As a merit of the joint network, the TAIJI mission could response to the alternative polarizations with a better antenna pattern in this case and observe these polarizations with a higher sensitivity. A caveat is that the different choices about the source location and/or merger time may yield a different constraints on the ppE parameters.

V. CONCLUSIONS

In this work, we explore the detectability of the LISA-TAIJI network to the alternative polarization modes compared to that of the single LISA mission. The ppE formulation is employed to specify the parameters $(\beta, b, \alpha_{\rm b}, \alpha_{\rm L}, \alpha_{\rm x}, \alpha_{\rm y})$ to be determined. To perform the investigations, two sources are selected, which are source1 $(m_1 = 10^5\ M_\odot, q = 1/3)$ at redshift $z = 2$, and source2 $(m_1 = 10^6\ M_\odot, q = 1/3)$ at the same distance. By using the Fisher matrix algorithm, for the last one year to coalescence, the ppE parameters are generally better measured from the source1 observation than the source2.

The joint LISA-TAIJI network could improve the measurement of β and b by a factor of ~ 2 compared to the single LISA mission. The joint observations show the significant improvement for the uncertainty of the alternative polarization modes coefficients α_i, and the joint network could reduce the uncertainty of the α_i by a factor of $\gtrsim 10$ compared to LISA, except $\gtrsim 4$ for $\alpha_{\rm b}$. In an optimistic scenario, if the location of the source is determined by the multimessenger observation, the joint LISA-TAIJI observation could further improve the measurement of the four coefficients of alternative polarization modes α_i, which should be an outcome of removing the degeneracies between the source distance and coefficients.

The current study employs the Fisher information matrix algorithm to determine the uncertainties of the ppE parameters with a single event, and only the approximate limits are achieved from this investigation. The Bayesian approaches have been proposed by Del Pozzo *et al.* [69] and Cornish *et al.* [56] to test the alternative gravitational theories. And more rigorous bounds could be obtained by applying the Bayesian algorithm to the LISA-TAIJI joint observation. We plan to perform these analyses in future studies.

ACKNOWLEDGMENTS

We thank Professor Wei-Tou Ni for helpful discussions and comments, and we also thank the anonymous referee for the constructive comments in helping us improve the manuscript. This work was supported by NSFC Grants No. 12003059 and No. 11773059, the Strategic Priority Research Program of the Chinese Academy of Sciences under Grant No. XDA15021102. This work made use of the High Performance Computing Resource in the Core Facility for Advanced Research Computing at Shanghai Astronomical Observatory.

APPENDIX: ANTENNA PATTEN OF A LISA-LIKE MISSION

For a LISA-like with full six functional links, the joint responses of three optimal TDI channels (A, E and T) represent the eventual response of the mission. And the response for the different GW polarization modes in the detector frame are shown in Fig. 9.

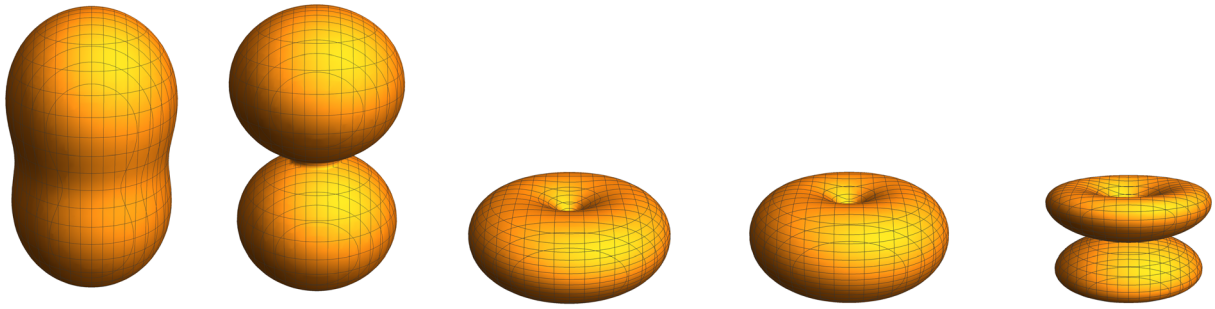

FIG. 9. The antenna pattern of joint LISA A + E + T channels for polarization modes tensor + (first plot), tensor × (second plot), scalar b/L (third plot), vector x (forth plot), and vector y (last plot) at 10 mHz in the detector frame.

[1] B. P. Abbott *et al.* (LIGO Scientific and Virgo Collaborations), GWTC-1: A Gravitational-Wave Transient Catalog of Compact Binary Mergers Observed by LIGO and Virgo during the First and Second Observing Runs, Phys. Rev. X **9**, 031040 (2019).

[2] R. Abbott *et al.* (LIGO Scientific and Virgo Collaborations), GWTC-2: Compact binary coalescences observed by LIGO and Virgo during the first half of the third observing Run, arXiv:2010.14527.

[3] B. P. Abbott *et al.* (LIGO Scientific and Virgo Collaborations), Tests of General Relativity with GW150914, Phys. Rev. Lett. **116**, 221101 (2016); Erratum, Phys. Rev. Lett. **121**, 129902 (2018).

[4] B. P. Abbott *et al.* (LIGO Scientific and Virgo Collaborations), Tests of general relativity with the binary black hole signals from the LIGO-Virgo catalog GWTC-1, Phys. Rev. D **100**, 104036 (2019).

[5] R. Abbott *et al.* (LIGO Scientific and Virgo Collaborations), Tests of general relativity with binary black holes from the second LIGO-Virgo gravitational-wave transient catalog, arXiv:2010.14529.

[6] C. Brans and R. H. Dicke, Mach's principle and a relativistic theory of gravitation, Phys. Rev. **124**, 925 (1961).

[7] C. M. Will, The Confrontation between general relativity and experiment, Living Rev. Relativity **17**, 4 (2014).

[8] C. M. Will, *Theory and Experiment in Gravitational Physics* (Cambridge University Press, Cambridge, 1993).

[9] T. Jacobson and D. Mattingly, Einstein-Aether waves, Phys. Rev. D **70**, 024003 (2004).

[10] J. D. Bekenstein, Relativistic gravitation theory for the modified Newtonian dynamics paradigm, Phys. Rev. D **70**, 083509 (2004).

[11] N. Rosen, Theory of gravitation, Phys. Rev. D **3**, 2317 (1971).

[12] N. Rosen, A theory of gravitation, Ann. Phys. (N.Y.) **84**, 455 (1974).

[13] A. P. Lightman and D. L. Lee, New two-metric theory of gravity with prior geometry, Phys. Rev. D **8**, 3293 (1973).

[14] K. Chatziioannou, N. Yunes, and N. Cornish, Model-independent test of general relativity: An extended post-Einsteinian framework with complete polarization content, Phys. Rev. D **86**, 022004 (2012).

[15] B. P. Abbott *et al.* (LIGO Scientific and Virgo Collaborations), GW170814: A Three-Detector Observation of Gravitational Waves from a Binary Black Hole Coalescence, Phys. Rev. Lett. **119**, 141101 (2017).

[16] B. P. Abbott *et al.* (LIGO Scientific and Virgo Collaborations), Tests of General Relativity with GW170817, Phys. Rev. Lett. **123**, 011102 (2019).

[17] H. Takeda, A. Nishizawa, Y. Michimura, K. Nagano, K. Komori, M. Ando, and K. Hayama, Polarization test of gravitational waves from compact binary coalescences, Phys. Rev. D **98**, 022008 (2018).

[18] H. Takeda, A. Nishizawa, K. Nagano, Y. Michimura, K. Komori, M. Ando, and K. Hayama, Prospects for gravitational-wave polarization tests from compact binary mergers with future ground-based detectors, Phys. Rev. D **100**, 042001 (2019).

[19] Y. Hagihara, N. Era, D. Iikawa, A. Nishizawa, and H. Asada, Constraining extra gravitational wave polarizations with Advanced LIGO, Advanced Virgo, and Kagra and upper bounds from GW170817, Phys. Rev. D **100**, 064010 (2019).

[20] H. Takeda, S. Morisaki, and A. Nishizawa, Pure polarization test of GW170814 and GW170817 using waveforms consistent with modified theories of gravity, arXiv:2010.14538.

[21] T. Akutsu, M. Ando, and E. A. Arai (KAGRA Collaboration), Overview of KAGRA: KAGRA science, arXiv:2008.02921.

[22] P. Amaro-Seoane, H. Audley, S. Babak *et al.* (LISA Team Collaboration), Laser Interferometer Space Antenna, arXiv:1702.00786.

[23] W.-R. Hu and Y.-L. Wu, The Taiji program in space for gravitational wave physics and the nature of gravity, Natl. Sci. Rev. **4**, 685 (2017).

[24] J. Luo *et al.* (TianQin Team Collaboration), TianQin: A space-borne gravitational wave detector, Classical Quant. Grav. **33**, 035010 (2016).

[25] A. Nishizawa, A. Taruya, and S. Kawamura, Cosmological test of gravity with polarizations of stochastic gravitational waves around 0.1–1 Hz, Phys. Rev. D **81**, 104043 (2010).

[26] M. Isi, A. J. Weinstein, C. Mead, and M. Pitkin, Detecting beyond-Einstein polarizations of continuous gravitational waves, Phys. Rev. D **91**, 082002 (2015).
[27] W.-H. Ruan, C. Liu, Z.-K. Guo, Y.-L. Wu, and R.-G. Cai, The LISA-Taiji network, Nat. Astron. **4**, 108 (2020).
[28] G. Wang, W.-T. Ni, W.-B. Han, S.-C. Yang, and X.-Y. Zhong, Numerical simulation of sky localization for LISA-TAIJI joint observation, Phys. Rev. D **102**, 024089 (2020).
[29] H. Omiya and N. Seto, Searching for anomalous polarization modes of the stochastic gravitational wave background with LISA and Taiji, Phys. Rev. D **102**, 084053 (2020).
[30] G. Orlando, M. Pieroni, and A. Ricciardone, Measuring Parity Violation in the Stochastic Gravitational Wave Background with the LISA-Taiji network, arXiv:2011.07059.
[31] C. Liu, W.-H. Ruan, and Z.-K. Guo, Constraining gravitational-wave polarizations with Taiji, Phys. Rev. D **102**, 124050 (2020).
[32] P. C. Peters and J. Mathews, Gravitational radiation from point masses in a Keplerian orbit, Phys. Rev. **131**, 435 (1963).
[33] P. C. Peters, Gravitational radiation and the motion of two point masses, Phys. Rev. **136**, B1224 (1964).
[34] S. Husa, Michele Maggiore: Gravitational waves. Volume 1: Theory and experiments, Gen. Relativ. Gravit. **41**, 1667 (2009).
[35] K. S. Thorne and C. M. Will, Theoretical frameworks for testing relativistic gravity. I. Foundations, Astrophys. J. **163**, 595 (1971).
[36] C. M. Will, Theoretical frameworks for testing relativistic gravity. 2. Parametrized post-Newtonian hydrodynamics, and the Nordtvedt effect, Astrophys. J. **163**, 611 (1971).
[37] W.-T. Ni, Theoretical frameworks for testing relativistic gravity. iv. A compendium of metric theories of gravity and their post-Newtonian limits, Astrophys. J. **176**, 769 (1972).
[38] N. Yunes and F. Pretorius, Fundamental theoretical bias in gravitational wave astrophysics and the parametrized post-Einsteinian framework, Phys. Rev. D **80**, 122003 (2009).
[39] K. Chatziioannou, N. Yunes, and N. Cornish, Model-independent test of general relativity: An extended post-einsteinian framework with complete polarization content, Phys. Rev. D **86**, 022004 (2012); Erratum, Phys. Rev. D **95**, 129901 (2017).
[40] G. Wang and W.-T. Ni, Numerical simulation of time delay interferometry for TAIJI and new LISA, Res. Astron. Astrophys. **19**, 058 (2019).
[41] G. Wang, W.-T. Ni, W.-B. Han, and C.-F. Qiao, Algorithm for TDI numerical simulation and sensitivity investigation, arXiv:2010.15544.
[42] M. Vallisneri and C. R. Galley, Non-sky-averaged sensitivity curves for space-based gravitational-wave observatories, Classical Quant. Grav. **29**, 124015 (2012).
[43] M. Otto, G. Heinzel, and K. Danzmann, TDI and clock noise removal for the split interferometry configuration of LISA, Classical Quant. Grav. **29**, 205003 (2012).
[44] M. Otto, Time-delay interferometry simulations for the laser interferometer space antenna, Ph.D. thesis, Gottfried Wilhelm Leibniz Universität Hannover (2015), https://www.repo.uni-hannover.de/handle/123456789/8598?locale-attribute=en.
[45] M. Tinto and O. Hartwig, Time-delay interferometry and clock-noise calibration, Phys. Rev. D **98**, 042003 (2018).
[46] T. A. Prince, M. Tinto, S. L. Larson, and J. W. Armstrong, The LISA optimal sensitivity, Phys. Rev. D **66**, 122002 (2002).
[47] M. Vallisneri, J. Crowder, and M. Tinto, Sensitivity and parameter-estimation precision for alternate LISA configurations, Classical Quant. Grav. **25**, 065005 (2008).
[48] F. B. Estabrook and H. D. Wahlquist, Response of Doppler spacecraft tracking to gravitational radiation, Gen. Relativ. Gravit. **6**, 439 (1975).
[49] H. Wahlquist, The Doppler response to gravitational waves from a binary star source, Gen. Relativ. Gravit. **19**, 1101 (1987).
[50] M. Tinto and M. E. da Silva Alves, LISA sensitivities to gravitational waves from relativistic metric theories of gravity, Phys. Rev. D **82**, 122003 (2010).
[51] S. Khan, S. Husa, M. Hannam, F. Ohme, M. Pürrer, X. J. Forteza, and A. Bohé, Frequency-domain gravitational waves from nonprecessing black-hole binaries. II. A phenomenological model for the advanced detector era, Phys. Rev. D **93**, 044007 (2016).
[52] Z. Luo, Z. Guo, G. Jin, Y. Wu, and W. Hu, A brief analysis to Taiji: Science and technology, Results Phys. **16**, 102918 (2020).
[53] G. Wang, W.-T. Ni, and W.-B. Han, Sensitivity investigation for unequal-arm LISA and TAIJI: The first-generation time-delay interferometry optimal channels, arXiv:2008.05812.
[54] C. Zhang, Q. Gao, Y. Gong, D. Liang, A. J. Weinstein, and C. Zhang, Frequency response of time-delay interferometry for space-based gravitational wave antenna, Phys. Rev. D **100**, 064033 (2019).
[55] B. F. Schutz, Networks of gravitational wave detectors and three figures of merit, Classical Quant. Grav. **28**, 125023 (2011).
[56] N. Cornish, L. Sampson, N. Yunes, and F. Pretorius, Gravitational wave tests of general relativity with the parameterized post-Einsteinian framework, Phys. Rev. D **84**, 062003 (2011).
[57] C. Cutler and É. E. Flanagan, Gravitational waves from merging compact binaries: How accurately can one extract the binary's parameters from the inspiral waveform?, Phys. Rev. D **49**, 2658 (1994).
[58] C. Cutler, Angular resolution of the LISA gravitational wave detector, Phys. Rev. D **57**, 7089 (1998).
[59] M. Vallisneri, Use and abuse of the Fisher information matrix in the assessment of gravitational-wave parameter-estimation prospects, Phys. Rev. D **77**, 042001 (2008).
[60] K. A. Kuns, H. Yu, Y. Chen, and R. X. Adhikari, Astrophysics and cosmology with a deci-hertz gravitational-wave detector: TianGO, Phys. Rev. D **102**, 043001 (2020).
[61] C. M. Will, Bounding the mass of the graviton using gravitational wave observations of inspiralling compact binaries, Phys. Rev. D **57**, 2061 (1998).
[62] C. M. Will and N. Yunes, Testing alternative theories of gravity using LISA, Classical Quant. Grav. **21**, 4367 (2004).
[63] E. Berti, A. Buonanno, and C. M. Will, Testing general relativity and probing the merger history of massive black holes with LISA, Classical Quant. Grav. **22**, S943 (2005).

[64] A. Stavridis and C. M. Will, Bounding the mass of the graviton with gravitational waves: Effect of spin precessions in massive black hole binaries, Phys. Rev. D **80**, 044002 (2009).

[65] K. G. Arun and C. M. Will, Bounding the mass of the graviton with gravitational waves: Effect of higher harmonics in gravitational waveform templates, Classical Quant. Grav. **26**, 155002 (2009).

[66] D. Keppel and P. Ajith, Constraining the mass of the graviton using coalescing black-hole binaries, Phys. Rev. D **82**, 122001 (2010).

[67] K. Yagi and T. Tanaka, Constraining alternative theories of gravity by gravitational waves from precessing eccentric compact binaries with LISA, Phys. Rev. D **81**, 064008 (2010); Erratum, Phys. Rev. D **81**, 109902 (2010).

[68] N. Yunes and S. A. Hughes, Binary pulsar constraints on the parameterized post-Einsteinian framework, Phys. Rev. D **82**, 082002 (2010).

[69] W. Del Pozzo, J. Veitch, and A. Vecchio, Testing general relativity using Bayesian model selection: Applications to observations of gravitational waves from compact binary systems, Phys. Rev. D **83**, 082002 (2011).